Eur. Phys. J. D **15**, 165–172 (2001)

THE EUROPEAN PHYSICAL JOURNAL D

EDP Sciences

Binary theory of antiproton stopping

P. Sigmund[1] and A. Schinner[2]

[1] Physics Department, Odense University (SDU), 5230 Odense M, Denmark
[2] Institut für Experimentalphysik, Johannes-Kepler-Universität, 4040 Linz-Auhof, Austria

Received 22 February 2001

Abstract. Binary theory of electronic stopping, developed recently with the aim of quantifying stopping forces on swift heavy ions, has been applied to antiproton stopping. Essential ingredients in the theory are inverse-Bloch and shell corrections. The numerical input consists of the excitation spectrum of the stopping material, characterized by bundled oscillator strengths extracted from tabulated optical properties. Predicted stopping forces for eight solid materials agree well with experimental data, in particular for Si where measurements span over two decades of projectile energy. Large discrepancies were found with stopping data for helium extracted from annihilation time measurements.

PACS. 34.50.Bw Energy loss and stopping power – 25.43.+t Antiproton-induced reactions – 29.30.Lw Nuclear orientation devices – 52.40.Mj Particle beam interactions in plasmas

1 Introduction

Experimental data on the stopping of keV and low-MeV antiprotons penetrating through matter have been compiled during the past decade [1–9]. Apart from the need for slowing-down data in antiproton physics, the initial motivation for such measurements was to clarify the Barkas effect, *i.e.*, the difference in stopping between a particle and its antiparticle. Early theoretical predictions of this effect differed by up to a factor of two from each other [10–13].

While that discrepancy was settled long ago it has become clear that the stopping of antiprotons is a particularly "clean" scattering problem from a theoretical point of view [14]: in the absence of bound projectile states the stopping process is dominated by Coulomb excitation of target electrons whereas projectile screening and antiscreening as well as electron capture and loss or projectile excitation do not complicate the matter as they may for positively charged particles. Therefore, accurate measurements of antiproton stopping provide a particularly stringent test on central aspects of stopping theory.

The basic simplicity of the stopping mechanism is in striking contrast with the observation that the agreement between theoretically predicted and measured antiproton stopping forces is little more than qualitative. An extensive bibliography of the theoretical literature over the past decade may be found in reference [15]. Explicit comparisons with experimental data have been performed on the basis of electron-gas models [15–19], the harmonic-oscillator model [9,17,20,21], and three mutually complementary quantal scattering models [22]. The best agreement, $\sim 10\%$, has been reached for silicon and aluminium [9,15,17,18,20]. For heavier solids [9,21] and for gas targets [22] much larger discrepancies were found. For Ag and Ti theoretical estimates were not even available [9]. It has been noted [14,23] that part of the problem with gas targets [5–7] may be inherent in the experimental method.

Theoretical schemes employed in estimates of antiproton stopping typically invoke elaborate quantal computations. Since Coulomb excitation of target electrons up to projectile energies ~ 100 keV/u should be well characterized by a classical-orbit picture [24] and since the Barkas effect is basically a classical polarization phenomenon [11] it appears tempting to explore the merits of classical stopping theory in this context, duly appended by a quantal correction where necessary.

We have recently developed a binary theory of stopping [25] geared toward ions heavier than helium in the classical regime. Allowance for an "inverse-Bloch correction" [26] was found to expand the range of validity of the theory into the Born regime, both for helium projectiles and for heavier ions beyond the Bohr limit [27,28]. The present paper is devoted to exploring the capability of that scheme to quantify antiproton stopping.

2 Fundamentals

In conventional terms the stopping force on a charged particle may be written as

$$-\frac{\mathrm{d}E}{\mathrm{d}x} = \frac{4\pi Z_1^2 Z_2 e^4}{mv^2} NL, \tag{1}$$

where Z_1 and Z_2 denote the atomic number of projectile and target, respectively ($Z_1 = -1$ for antiprotons), N the

number of target atoms per volume and v the projectile speed. The essential physics is contained in the dimensionless stopping number L which we write as

$$L = L_0 + L_1 + L_{\text{Bloch}}, \tag{2}$$

the three terms on the right-hand side being defined as follows,

- L_0 is independent of Z_1 and the leading term in a quantal perturbation series in Z_1 (Bethe theory or equivalent). As a matter of definition, L_0 is meant to incorporate shell corrections, *i.e.*, to fully account for intrinsic motion of target electrons,
- L_1 denotes the Barkas correction which depends on the sign of Z_1 and is meant to go beyond first order in Z_1 when necessary,
- L_{Bloch} denotes the Bloch correction which is small in the Born regime ($v > 2Z_1 v_0$, v_0 = Bohr velocity) but substantial in the classical regime.

Equation (2) ignores processes involving bound projectile states which might have to be allowed for in case of protons. Moreover a correction for recoil processes (nuclear stopping) is necessary at very low energies and easily estimated by standard procedures.

The standard form of the Bloch term reads [29,30]

$$L_{\text{Bloch}} = -\gamma - \Re\psi\left(1 - \mathrm{i}\frac{Z_1 e^2}{\hbar v}\right), \tag{3}$$

where ψ denotes the logarithmic derivative of the gamma function and $\gamma = 0.5772$ is Euler's constant. The lack of shell corrections in this expression is potentially serious at low velocities and has to be kept in mind.

As long as shell corrections are neglected, L_0 reduces to the Bethe logarithm [31]

$$L_0 \longrightarrow \ln\frac{2mv^2}{\hbar\omega}, \tag{4}$$

where $\omega = I/\hbar$ is a resonance frequency of the target and I the mean excitation energy or "I-value". Under the same assumption $L_0 + L_{\text{Bloch}}$ reduces to the Bohr logarithm

$$L_{\text{Bohr}} \to \ln\frac{Cmv^3}{Z_1 e^2 \omega}; \qquad C = 2\mathrm{e}^{-\gamma} = 1.1229 \tag{5}$$

in the low-speed limit.

The stopping number L, when written in the form of equation (2), reduces to L_0 in the high-speed limit. As an alternative we now write

$$L = L_{\text{bin}} + \Delta L, \tag{6}$$

where L_{bin} denotes the prediction of the binary theory outlined in reference [25] while ΔL denotes a correction term. Being based on classical theory, L_{bin} describes the low-speed behavior while the correction term ΔL becomes important at high projectile speed. We note that L_{bin} has been found to incorporate a reasonable Barkas correction [25], and a classical shell correction [32] can be allowed for *via* kinetic theory [28,33].

From equations (2) and (6) we obtain

$$\Delta L = L_0 - L_{\text{bin}} + L_1 + L_{\text{Bloch}} \tag{7}$$

which reduces to

$$\begin{aligned}\Delta L &\overset{v\ \text{high}}{\to} \ln\frac{2mv^2}{\hbar\omega} - \ln\frac{Cmv^3}{Z_1 e^2\omega} - \gamma - \Re\psi\left(1 - \mathrm{i}\frac{Z_1 e^2}{\hbar v}\right)\\ &\equiv \ln\frac{Z_1 e^2}{\hbar v} - \Re\psi\left(1 - \mathrm{i}\frac{Z_1 e^2}{\hbar v}\right)\end{aligned} \tag{8}$$

in the high-speed limit where Barkas and shell corrections become negligible.

Equation (8) defines the inverse-Bloch correction mentioned in reference [26], a quantum correction to the binary theory ensuring proper approach to the Bethe formula at high speed. We need to extend equation (8) into the nonasymptotic region; hence a shell correction has to be applied. Since the Bloch correction is a binary-collision effect [30] that shell correction can be determined accurately from kinetic theory [33].

In principle another term would have to be added to equation (8), accounting for differences in the Barkas correction between classical and quantum theory. We have found for the case of lithium ions in carbon [34] that this difference is negligibly small around the stopping maximum. No such correction has been included in the present scheme.

At moderate and low projectile speed a single excitation frequency ω is known to be inadequate to characterize the target. It is then necessary to allow for the excitation spectrum with frequencies ω_j weighted by the dipole oscillator strengths f_j which are normalized according to $\sum_j f_j = 1$. With this, stopping forces may be computed from the expression

$$L = \sum_j f_j \{L_{\text{bin},j} + \Delta L_j\}_j, \tag{9}$$

where the symbol $\{\dots\}_j$ denotes the shell correction operator in kinetic theory [33],

$$\{L_j\}_j = v\int \mathrm{d}^3 v_{\mathrm{e}}\, g_j(v_{\mathrm{e}})\,\frac{\mathbf{v}\cdot(\mathbf{v}-\mathbf{v}_{\mathrm{e}})}{|\mathbf{v}-\mathbf{v}_{\mathrm{e}}|^3}\,L_j(|\mathbf{v}-\mathbf{v}_{\mathrm{e}}|), \tag{10}$$

$g_j(v_{\mathrm{e}})$ represents the velocity distribution of target electrons in the jth shell or subshell and $L_j(v)$ the stopping number of the jth target shell neglecting orbital velocities $\mathbf{v}_{\mathrm{e}}$.

3 Binary theory

For details on binary stopping theory the reader is referred to [25]. The essential feature is the replacement of binding of target electrons by screening of the projectile-target interaction. This reduces the interaction to a binary scattering process which, to a high degree of rigor, is characterized by a Yukawa potential with the adiabatic radius

taken as the screening radius. The scheme considers transfer of both kinetic and potential energy.

For antiprotons, as for all point projectiles, the theory is asymptotically equivalent to the Bohr theory [35] both in the limit of close and distant collisions. A smooth function characterizes the energy loss at intermediate impact parameters. Since no perturbation expansion is invoked, higher-order Z_1 terms are incorporated which were found to be close to – yet not identical with – the known Z_1^3-term at large impact parameters. Systematic comparisons with measured stopping forces on heavier ions – which are known to be sensitive to input on higher-order Z_1 terms [34] – indicate that predictions of the binary theory concerning these corrections are competitive [27,28,36].

4 Input

Binary theory determines stopping numbers $L_{\mathrm{bin},j}$ entering into equation (9), *i.e.*, ignoring the orbital motion of target electrons. The prime numerical input is a set of (f_j, ω_j) pairs. The choice of those pairs does not only affect stopping forces on antiprotons but also predictions on stopping of heavy ions by the respective targets. Therefore we take this opportunity to specify our procedure – which has been guided by previous work of Mikkelsen [20,41] – in some detail.

Oscillator-strength spectra over a very wide energy range can be extracted from tabulations of optical constants [37,38] and X-ray scattering factors [39]. The reliability of spectra extracted from either source was tested primarily *via* f-sum rule and I-value. While spectra evaluated from X-ray data consistently passed this test we were unable to extract reliable spectra from references [37,38] alone for several materials including Cu and Ag. Therefore we adopted spectra extracted from reference [39] for the solid materials over the full tabulated energy range, 29.3 eV $\leq E \leq$ 30 000 eV. Data from references [37,38] were employed for $E <$ 29.3 eV.

For high-Z_2 atoms the spectrum may extend significantly beyond 30 000 eV. The choice of procedure applied here affects the f-sum rule and in particular the calculated I-value but has no visible influence on antiproton stopping in the velocity range considered here. For moderately large Z_2 such as for copper where the K-absorption edge lies below 30 000 eV, the power law obeyed by $f(E)$ was extrapolated to higher energies. For high-Z_2 atoms (Ta, Pt and Au), the power law obeyed by $f(E)$ within the L shell was extrapolated up to the K absorption edge and contributions from the K shell were ignored. This results in a violation of the f-sum rule and in a significant underestimate of the I-value as compared to recommended values [40][1].

[1] For consistency we have defined $I = \hbar\omega$ in accordance with equation (12), with integration limits comprising the entire data range in those cases where the f-sum rule was not fulfilled. This definition does not affect our calculated stopping forces but is relevant in a comparison with tabulated I-values.

Continuous spectra found in this way were then bundled according to

$$f_j = \int_{\omega_{j1}}^{\omega_{j2}} \mathrm{d}\omega f(\omega) \tag{11}$$

$$\ln \omega_j = \frac{1}{f_j} \int_{\omega_{j1}}^{\omega_{j2}} \mathrm{d}\omega f(\omega) \ln \omega. \tag{12}$$

Our choice of upper and lower limit ω_{j2} and ω_{j1}, respectively, was guided by absorption edges, nominal occupation numbers of shells and subshells, and the grid of the tabulated data. The lower limit ω_{j1} for a principal shell was placed at an absorption edge whenever its position was obvious from the spectrum, *i.e.*, for inner shells. The remaining spectrum was then divided into principal shells in rough accordance with the nominal occupation numbers. Since the scheme is rather insensitive to the precise choice of these limits – examples will be discussed below – and since this division was done manually by trial-and-error, deviations in $f_j Z_2$ from nominal occupation numbers up to ± 0.5 were tolerated. A somewhat greater difference was accepted in case of Ag (*cf.* below).

With the exception of Ta and Pt and one each of the spectra for Ag and Au, f_j was renormalized to fulfill the f-sum rule. The necessary change was at the few % level in all cases.

Quite good agreement with measured stopping forces has been found when the j-grid just reflected the principal shells. Division into ℓ-subshells constitutes an improvement mainly because shell corrections depend on the angular-momentum quantum number ℓ. Despite extensive tests we have never identified discernible effects of grids finer than the subshell level. At high projectile speed this must be so since only the I-value enters the stopping force. At low velocities the shell correction expressed by equation (10) tends to smear out all structure over a broad interval [33].

Two procedures were applied to allow for ℓ-dependent shell corrections. The simplest is to operate with an effective ℓ-value for each principal shell, chosen as the integer closest to the average ℓ-value. The second is subshell splitting which has been found significant only for outer shells and was carried out in several cases, again with a tolerance level of ± 0.5 in $f_j Z_2$.

The lower limit ω_{j1} for the jth shell or subshell also acts as the binding energy, *i.e.*, the maximum amount of *potential*-energy transfer to an electron in the respective shell/subshell [25]. This is the obvious choice whenever ω_{j1} coincides with an absorption edge and a reasonable operational definition otherwise.

In a few test cases input data were taken over from [41].

Tables 1–4 show spectra employed for nine materials. Two alternative choices were studied for Si, Al, Cu, Ag, Au and He (Tabs. 1 and 4).

Spectra for Si and Al are taken over from [41], and the two versions differ only in the subshell division. The ratio of the f-values in the version to the left is that of the nominal number of electrons in those subshells.

Table 1. Target spectra adopted for silicon, aluminium, copper, silver and gold.

(n,ℓ)	$Z_2 f$	$\hbar\omega$ (eV)	$Z_2 f$	$\hbar\omega$ (eV)
$_{14}$Si	5 shells		3 shells	
$(1,0)$	1.711	3178.62	1.711	3178.62
$(2,0)$	2.090	248.90	8.361	248.90
$(2,1)$	6.271	248.90		
$(3,0)$	1.964	20.26	3.928	20.26
$(3,1)$	1.964	20.26		
Atom	14.000	168.08	14.000	168.08
$_{13}$Al	5 shells		3 shells	
$(1,0)$	1.753	2795.47	1.753	2795.47
$(2,0)$	2.076	201.96	8.304	201.96
$(2,1)$	6.228	201.96		
$(3,0)$	1.962	16.89	2.943	16.89
$(3,1)$	0.981	16.89		
Atom	13.000	164.14	13.000	164.14
$_{29}$Cu	6 shells		4 shells	
$(1,0)$	1.454	15185.0	1.479	15716.0
$(2,1)$	8.050	1667.3	7.963	1667.2
$(3,0)$	1.932	606.05		
$(3,1)$	6.316	249.03	17.667	147.5
$(3,2)$	10.154	74.41		
$(4,0)$	1.094	16.96	1.620	19.905
Atom	29.000	325.9	29.000	328.14
$_{47}$Ag	Incomplete		Extrapolated	
$(1,0)$	0.324	27538	1.578	45840.0
$(2,1)$	6.309	5825	6.142	5824.9
$(3,1)$	21.367	835.3	20.710	838.5
$(4,0)$	1.956	246.4	2.354	231.7
$(4,1)$	6.147	91.61	6.125	87.23
$(4,2)$	9.894	47.89	9.368	45.94
$(5,0)$	0.985	15.13	0.723	13.419
Atom	46.982	398.0	47.000	453.7
$_{79}$Au	7 shells		6 shells	
$(1,0)$			1.098	96235.0
$(2,1)$	5.084	20101.0	6.344	25918.0
$(3,1)$	19.498	3769.5	19.537	4116.0
$(4,2)$	32.353	594.19	33.416	599.0
$(5,0)$	2.392	150.35		
$(5,1)$	5.373	81.980	8.880	87.3
$(5,2)$	10.401	43.015		
$(6,0)$	0.978	15.015	9.725	36.9
Atom	76.079	670.0	79.000	800.0

Table 2. Target spectrum adopted for titanium ($Z_2 = 22$).

(n,ℓ)	$Z_2 f$	$\hbar\omega$ (eV)
$(1,0)$	1.571	8549.9
$(2,1)$	8.290	850.59
$(3,0)$	2.089	242.32
$(3,1)$	6.027	67.185
$(3,2)$	2.020	37.318
$(4,0)$	2.003	14.987
Atom	22.000	230.7

Table 3. Target spectra for Ta and Pt. f-sum and I-value less than nominal values because of cutoff at 30 000 eV (see text).

	tantalum ($Z_2 = 73$)		platinum ($Z_2 = 78$)	
(n,ℓ)	$Z_2 f$	$\hbar\omega$ (eV)	$Z_2 f$	$\hbar\omega$ (eV)
$(2,1)$	6.035	19080.0	6.059	22244.0
$(3,1)$	19.324	3096.0	18.826	3745.0
$(4,2)$	32.929	415.21	31.870	623.86
$(5,1)$	10.545	57.114	19.110	69.803
$(6,0)$	2.804	20.398	0.599	14.174
Atom	71.637	654.1	76.464	723.0

Table 4. Target spectra adopted for helium ($Z_2 = 2$).

(n,ℓ)	$Z_2 f$	$\hbar\omega$ (eV)	$Z_2 f$	$\hbar\omega$ (eV)
	3 shells		1 shell	
$(1,0)$	0.442	22.0	2.000	41.8
$(1,0)$	1.482	49.0		
$(1,0)$	0.076	95.2		
Atom	2.000	42.14	2.000	41.8

The two options for Cu originate in two independent evaluations of the same continuous spectrum, including extrapolation of the K shell. The main difference is in the subshell splitting of the M shell.

Silver is the only material where the given continuous spectrum, with a K-shell portion feasibly extrapolated beyond 30 000 eV, yields an f-sum greater than $Z_2 = 47$. The two spectra represent two feasible ways of overcoming this problem. The one on the left avoids extrapolation and renormalization and, consequently, underestimates the contribution from the K shell. The spectrum on the right was found by extrapolation and subsequent renormalization.

The two spectra for gold differ significantly. The spectrum on the right is identical with the one employed in reference [9]. The one on the left was evaluated by the procedure described above with the K shell omitted and subshell splitting applied to the O shell.

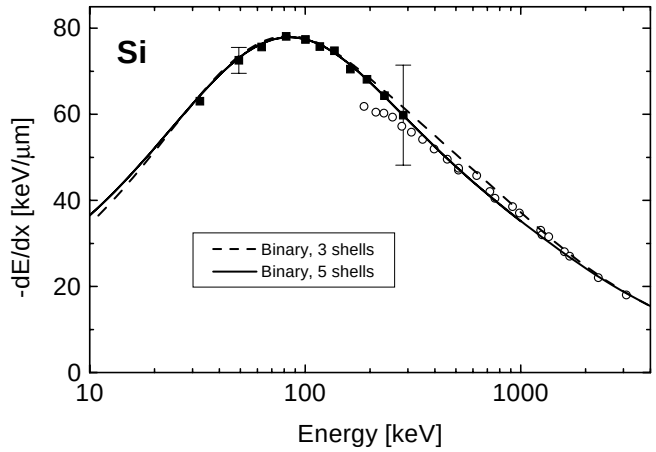

Fig. 1. Antiprotons in Si: calculations for two sets of input (Tab. 1) compared with experimental data from references [1,4,9].

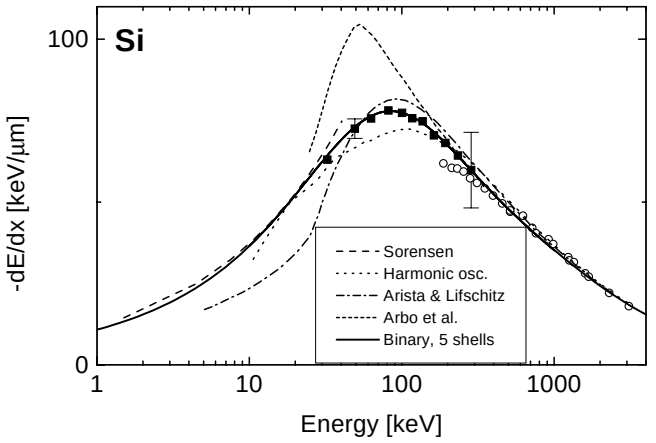

Fig. 2. Antiprotons in Si: comparison of theoretical predictions [9,15,16,19] with present estimate. Experimental data as in Figure 1.

Tables 2 and 3 show one spectrum each for Ti, Ta and Pt, the latter two being determined without inclusion of the K shell.

Table 4 shows two spectra for helium. The spectrum on the left was bundled from data compiled in reference [42] while the one on the right operates with a single resonance at the recommended frequency [40].

Velocity distributions of target electrons have been determined *via* Fourier transform of tabulated atomic wave functions [43] for the relevant subshells (n, ℓ) as reported previously [28].

5 Results

Figure 1 shows stopping forces in silicon calculated with input from Table 1 compared with measurements. Both the height and the position of the stopping maximum are predicted accurately for both sets of input parameters. The difference between the two predictions is small and noticeable mainly in the region above the stopping maximum.

Figure 2 includes theoretical predictions from the literature. The harmonic-oscillator model [9,20,41] shows quite good agreement except for a slight (∼10%) underestimate near the stopping maximum. This is consistent with the experience [34] that perturbation theory tends to overestimate the Barkas effect. The nonlinear theory of reference [15] shows a rather different behavior at low velocities where experimental data do not yet exist, while the close agreement of the binary prediction with the low-velocity results of reference [16] – based on a Fermi gas model – is striking.

Figure 3 shows the calculated stopping force and its contributions from the three principal target shells. It is seen that the contribution from the K shell amounts to up to 1% in the energy range where experimental data exist. The L shell contributes about 10% up to the stopping maximum and competes with the M shell above ∼ 1 MeV.

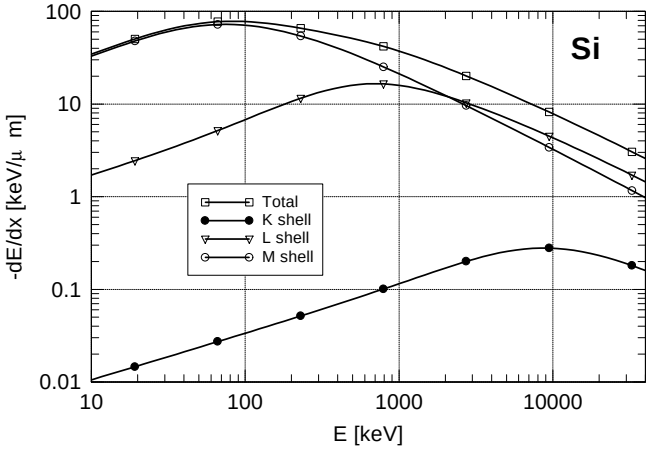

Fig. 3. Antiprotons in Si: contribution from principal target shells. Input from Table 1, right part.

Figures 4 and 5 show equivalent information for aluminium. Similar comments apply as for Si although experimental data cover a smaller energy interval. One more theoretical prediction [18] has been included in Figure 5 which is found to run in between those of the binary theory and of reference [15].

Figures 6–10 show similar comparisons for Ti, Cu, Ag, Ta and Pt. Good absolute agreement is found in all cases with the possible exception of a minor shift in the position of the maximum in case of copper for both of the spectra specified in Table 1. We note that despite some uncertainty in the spectrum for silver, the difference between the resulting predicted stopping forces is less than experimental error.

Figure 11 shows results for gold. It is seen that the two spectra specified in Table 1 lead to substantially different predictions for the stopping force. The main cause of the difference lies in the description of the two outer shells. The binary model with 6 shells comes close to the results of the harmonic-oscillator model, as could be expected in view of similar input. The binary model involving 7 shells

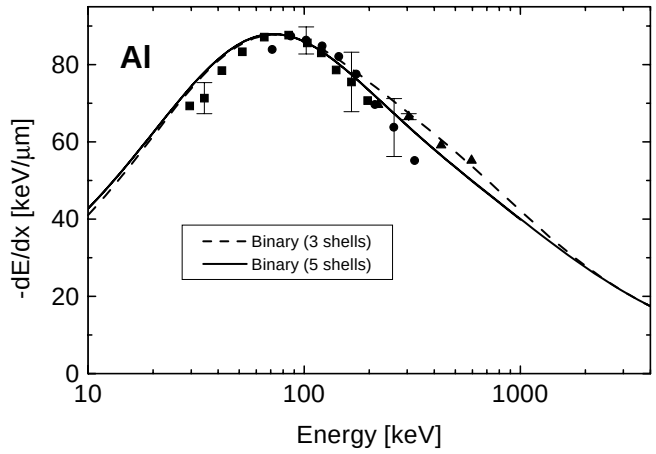

Fig. 4. Antiprotons in Al: calculations for two sets of input (Tab. 1) compared with experimental data from reference [9].

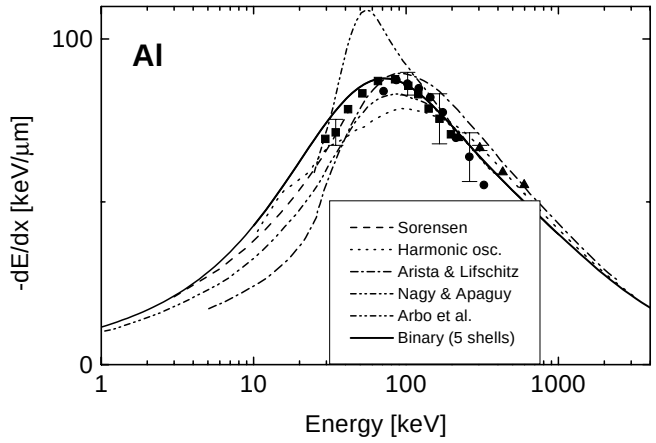

Fig. 5. Antiprotons in Al: comparison of theoretical predictions [9,15,16,18,19] with present estimate. Experimental data as in Figure 4.

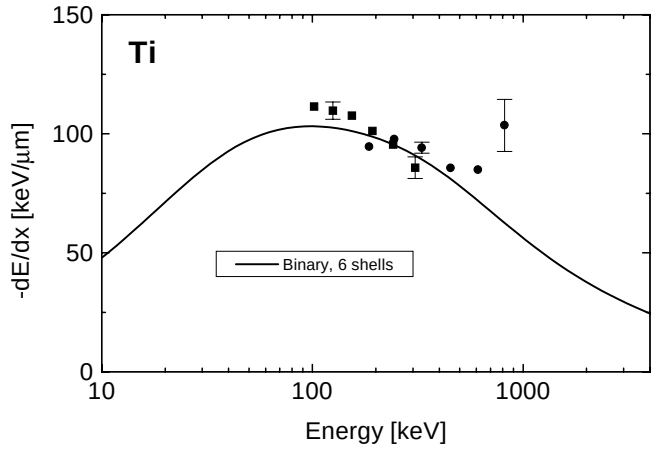

Fig. 6. Antiprotons in Ti: calculation with input from Table 2 compared with experimental data from reference [9].

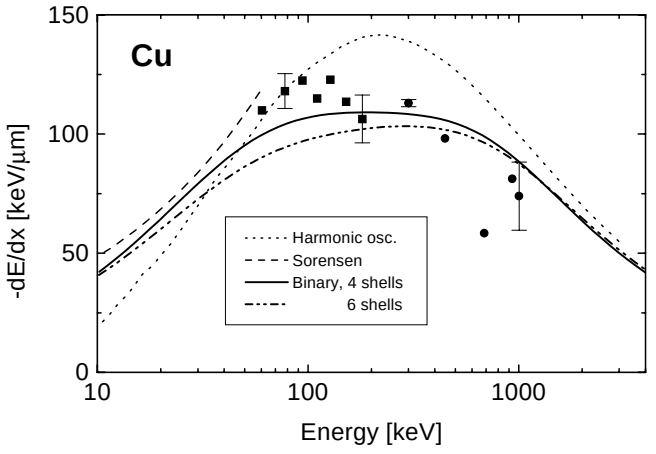

Fig. 7. Antiprotons in Cu: calculations with input from Table 2 compared with experimental data from reference [9] and previous theoretical estimates [9,16].

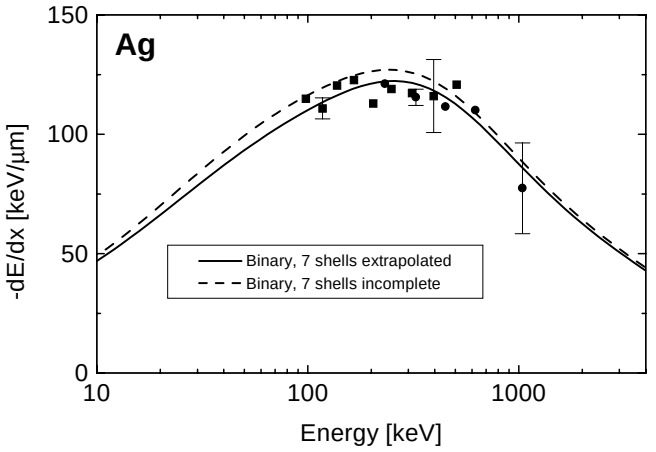

Fig. 8. Antiprotons in Ag: calculations with input from Table 2 compared with experimental data from reference [9].

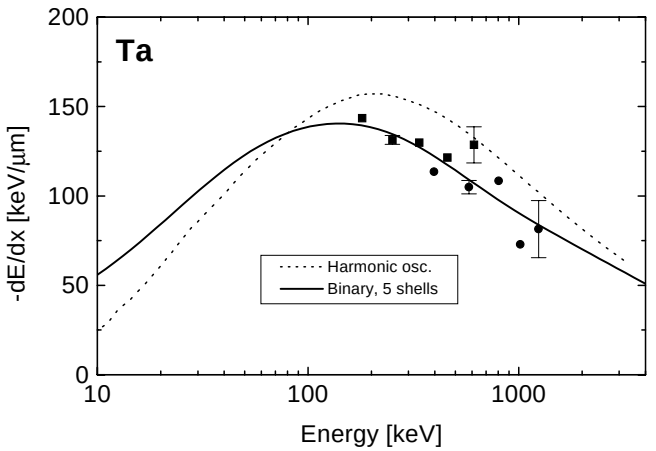

Fig. 9. Antiprotons in Ta: calculation with input from Table 3 compared with experimental data from reference [9] and a previous theoretical estimate [9].

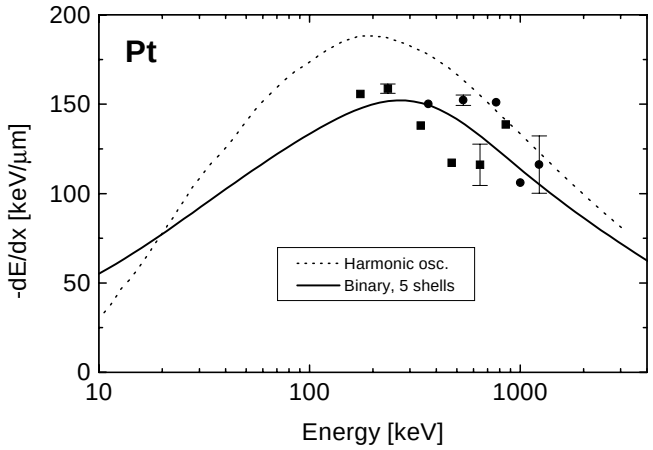

Fig. 10. Antiprotons in Pt: calculation with input from Table 3 compared with experimental data from reference [9] and a previous theoretical estimate [9].

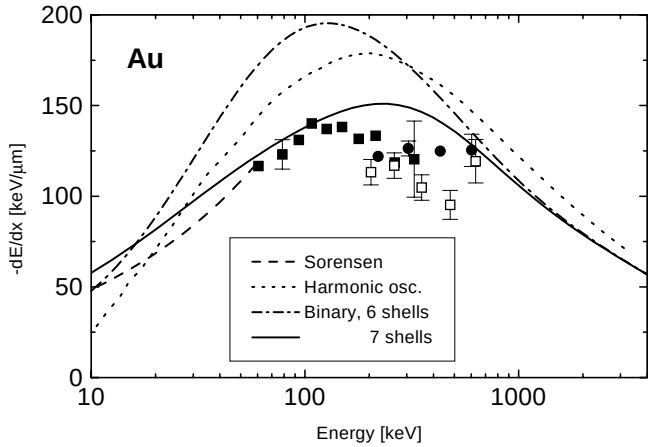

Fig. 11. Antiprotons in Au: comparison of two predictions of the binary theory with input from Table 1 with experimental [3,9] and previous theoretical estimates [9,16].

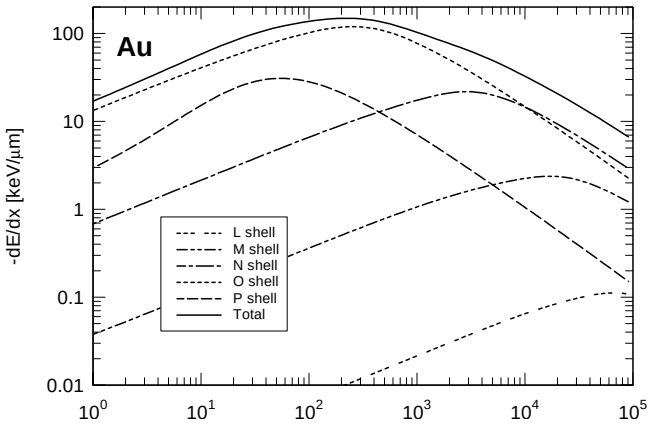

Fig. 12. Antiprotons in Au: contribution from principal shells. Input from an 11-shell model similar to the left part of Table 1.

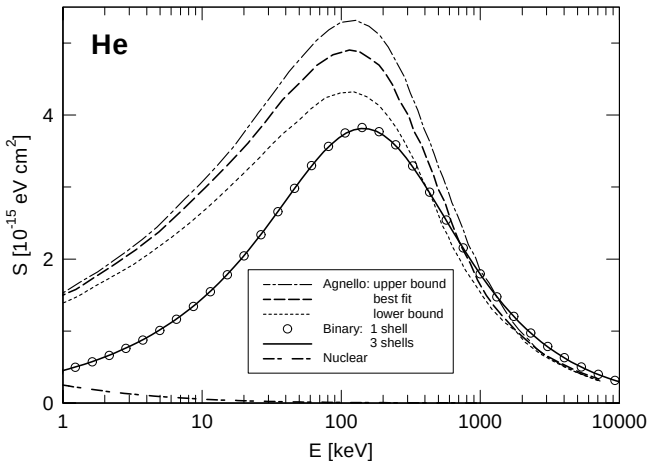

Fig. 13. Antiprotons in He: comparison of two predictions of the binary theory (Tab. 1) with results given in reference [6].

comes about as close to the experimental results as feasible, considering the scatter of experimental data. Again, there is very good agreement between our prediction and the result from the electron-gas model at low speed.

Figure 12, showing the contributions from the main shells, demonstrates the leading role of the O shell over the entire energy range where experimental data are available. This is due to the large number of electrons in that shell. Although the contribution from the single P electron shows a seemingly special energy dependence, it does approaches the common $\sqrt{E}$ variation at lower energies outside the interval covered by the graph.

Figure 13 shows a comparison between calculated stopping forces in helium and data extracted from measurements of the annihilation time of antiprotons as a function of gas pressure [6]. The complete agreement between the two binary results confirms our experience that subdivision of a spectrum beyond the subshell level does not cause a noticeable change. The agreement with the results of reference [6], on the other hand, is very poor. Although there is a noticeable contribution from nuclear stopping – which has been included in the graph – this cannot be the dominating cause of the discrepancy. In view of the good agreement with direct measurements documented above we believe that the present finding further supports the question marks at the experimental method set in references [9,14]. While it is hard to see how our calculations could be in error by almost a factor 3 at low speed, the discrepancy at the high-speed end, although smaller, appears even more serious because of the absence of a significant Barkas correction above 1 MeV.

6 Conclusion

We may conclude that the binary theory, duly appended by an inverse-Bloch correction and shell corrections, reproduces stopping forces on antiprotons in eight solid materials without the use of adjustable parameters over the entire velocity range for which measurements have been reported. The agreement with experimental data is within experimental uncertainty with the possible exception of

gold and copper. A particular strength of the theory is the explicit inclusion of electron binding, as opposed to free-electron models, the range of applicability of which is limited to light target materials for that reason. Unlike the harmonic-oscillator model, the binary theory allows for ℓ-dependent shell corrections. The resulting difference is subtle for Al and Si but substantial for Au.

One might put a question mark at the validity of shell corrections determined from atomic wave functions applied to conduction electrons, and one might argue that the Fermi distribution should lead to a superior description. Despite excellent agreement with the predictions of the Fermi-gas model at low velocities in Figures 2, 5, 7 and 11, representing a considerable variation in the outermost shell, we cannot exclude the possibility of this being the origin of minor discrepancies observed for copper and gold in Figures 7 and 11. Proper consideration of this point, however, would have to include attention to $3d$ and $5d$ electrons, respectively, which are much larger in number than the $4s$ and $6s$ electrons, respectively. This will eventually have to be done, but since we consider it to be a second-order effect, and since it will unquestionably affect the basic simplicity of the physical picture, this point will be reserved to a separate study.

From the point of view of the general theory of charged-particle stopping we find it gratifying that one and the same theoretical procedure can reproduce stopping forces for a wide variety of ions and energies. Moreover, the comparisons with experiment provide a most useful test on oscillator-strength spectra applied in estimates of heavy-ion stopping.

This work has been supported by the Danish Natural Science Research Council (SNF). We gratefully acknowledge valuable advice as well as originals of published data from Henning H. Mikkelsen and Søren P. Møller.

References

1. L.H. Andersen *et al.*, Phys. Rev. Lett. **62**, 1731 (1989).
2. G. Gabrielse *et al.*, Phys. Rev. A **40**, 481 (1989).
3. R. Medenwaldt *et al.*, Phys. Lett. A **155**, 155 (1991).
4. R. Medenwaldt *et al.*, Nucl. Instrum. Meth. **58**, 1 (1991).
5. A. Adamo *et al.*, Phys. Rev. A **47**, 4517 (1993).
6. M. Agnello *et al.*, Phys. Rev. Lett. **74**, 371 (1995).
7. A. Bertin *et al.*, Phys. Rev. A **54**, 5441 (1996).
8. S.P. Møller *et al.*, Nucl. Instrum. Meth. B **122**, 162 (1997).
9. S.P. Møller *et al.*, Phys. Rev. A **56**, 2930 (1997).
10. J.C. Ashley, R.H. Ritchie, W. Brandt, Phys. Rev. B **5**, 2393 (1972).
11. J. Lindhard, Nucl. Instrum. Meth. **132**, 1 (1976).
12. C.C. Sung, R.H. Ritchie, Phys. Rev. A **28**, 674 (1983).
13. H.H. Mikkelsen, P. Sigmund, Phys. Rev. A **40**, 101 (1989).
14. A.H. Sørensen, Phys. At. Nucl. **57**, 6 (1994).
15. N.R. Arista, A.F. Lifschitz, Phys. Rev. A **59**, 2719 (1999).
16. A.H. Sørensen, Nucl. Instrum. Meth. B **48**, 10 (1990).
17. H.H. Mikkelsen, H. Esbensen, P. Sigmund, Nucl. Instrum. Meth. B **48**, 8 (1990).
18. I. Nagy, B. Apagyi, Phys. Rev. A **58**, R1653 (1998).
19. D.G. Arbó, M.S. Gravielle, J.E. Miraglia, Phys. Rev. A **62**, 032901 (2000).
20. H.H. Mikkelsen, *Higher Order Effects in Electronic Stopping: The Oscillator Model*, Ph.D. thesis, Odense University (1990).
21. H.H. Mikkelsen, Nucl. Instrum. Meth. B **69**, 22 (1992).
22. G. Schiwietz, U. Wille, R.D. Muino, P.D. Fainstein, P.L. Grande, J. Phys. B **29**, 307 (1996).
23. S.P. Møller, *Experimental investigations of stopping power and straggling for very low and very high energy particles of positive and negative charge*, Dr. Sci. thesis, University of Aarhus (1998).
24. N. Bohr, Mat. Fys. Medd. Dan. Vid. Selsk. **18**, 1 (1948).
25. P. Sigmund, A. Schinner, Eur. Phys. J. D **12**, 425 (2000).
26. P. Sigmund, Phys. Rev. A **54**, 3113 (1996).
27. P. Sigmund, A. Schinner, Nucl. Instrum. Meth. B **174**, 535 (2001).
28. P. Sigmund, A. Schinner, Phys. Scripta (in press, 2001).
29. F. Bloch, Ann. Physik **16**, 285 (1933).
30. J. Lindhard, A.H. Sørensen, Phys. Rev. A **53**, 2443 (1996).
31. H. Bethe, Ann. Physik **5**, 324 (1930).
32. P. Sigmund, Eur. Phys. J. D **12**, 111 (2000).
33. P. Sigmund, Phys. Rev. A **26**, 2497 (1982).
34. A. Schinner, P. Sigmund, Nucl. Instrum. Meth. B **164-165**, 220 (2000).
35. N. Bohr, Philos. Mag. **25**, 10 (1913).
36. P. Sigmund, A. Schinner, in *Fundamental & Applied Aspects of Modern Physics* (World Scientific, in press).
37. E.D. Palik, *Handbook of Optical Constants of Solids*, Academic Press Handbook Series (Academic Press, Orlando, 1985), Vol. 1.
38. E.D. Palik, *Handbook of Optical Constants of Solids* (Academic Press, Boston, 1991), Vol. 2.
39. B.L. Henke, E.M. Gullikson, J.C. Davies, At. Data Nucl. Data Tables **54**, 181 (1993).
40. ICRU, *Stopping Powers and Ranges for Protons and Alpha Particles* (ICRU, International Commission of Radiation Units and Measurements, Bethesda, Maryland, 1994), Vol. 49.
41. H.H. Mikkelsen, unpublished (1997), quoted in [9].
42. E.H. Mortensen, *Stopping Power for Charged Particles in Atomic and Molecular Gases* (in *Danish*), M. Sci. thesis, Odense University, 1990.
43. E. Clementi, C. Roetti, At. Data Nucl. Data Tables **14**, 177 (1974).